UNDERSTANDING SELF-SUPERVISED LEARNING AS AN APPROXIMATION OF SUPERVISED LEARNING

Anonymous authors
Paper under double-blind review

ABSTRACT

Self-supervised representation learning has mainly advanced in an empirical rather than theoretical manner. Many successful algorithms combine multiple techniques that are supported by experiments. This approach makes it difficult for the community to understand self-supervised learning fundamentally. To help settle this situation, we take a principled approach. We theoretically formulate a self-supervised learning problem as an approximation of a supervised learning problem. From the formulated problem, we derive a loss that is closely related to existing contrastive losses, thereby providing a foundation for these losses. The concepts of prototype representation bias and balanced contrastive loss are naturally introduced in the derivation, which provide insights to help understand self-supervised learning. We discuss how components of our framework align with practices of self-supervised learning algorithms, focusing on SimCLR. We also investigate the impact of balancing the attracting force between positive pairs and the repelling force between negative pairs. The proofs of our theorems are provided in the appendix, and the code to reproduce experimental results is provided in the supplementary material.

1 INTRODUCTION

Representation learning, the process of acquiring condensed but meaningful representations, lies at the core of advancing machine learning capabilities. Conventional supervised learning depends heavily on labeled data. It can be problematic in the face of diverse and dynamic real-world data. Human annotation is not scalable due to its labor-intensive requirement and not generalizable due to its subjective nature. Furthermore, it is error-prone (Vasudevan et al., 2022; Beyer et al., 2020; Shankar et al., 2020).

Amidst these challenges, self-supervised learning has emerged as a new paradigm, supported by the notion that humans primarily learn from unlabeled data (Orhan et al., 2020; Savage, 2019). It has demonstrated success in various fields, including but not limited to computer vision, natural language processing, and speech recognition (Ozbulak et al., 2023; Schiappa et al., 2023; Gui et al., 2023).

However, unlike supervised learning, self-supervised learning has primarily been driven empirically, with limited emphasis on theoretical foundation.[1] The mainstream approach is to adopt Siamese networks as base architecture and combine various engineering techniques, such as memory banks, momentum encoders, stop-gradient, projectors, predictors, multi-crop, and centering (Wu et al., 2018; He et al., 2020; Grill et al., 2020; Chen & He, 2021; Caron et al., 2020; 2021; Purushwalkam & Gupta, 2020). The techniques are often explained intuitively, and their performance is supported by experiments. This approach may not be satisfactory since it can obscure what problem the algorithms are addressing essentially.

In this paper, we theoretically formulate a self-supervised learning problem and derive its solution. To do so, we observe that self-supervised learning is more nuanced compared to unsupervised learning. It not only utilizes unlabeled data but also generates its own labels from it.[2] This suggests a connection

[1] Self-supervised learning is sometimes metaphorically referred to as the dark matter of intelligence, implying that its principle is not easily understood despite its significant impact (Balestriero et al., 2023).

[2] This is implied within expressions such as pseudo labels (Doersch et al., 2015; Noroozi & Favaro, 2016; Zhang et al., 2016; Gidaris et al., 2018), target (or teacher) encoders (Tarvainen & Valpola, 2017; He et al., 2020; Grill et al., 2020; Chen & He, 2021; Caron et al., 2021; Oquab et al., 2023) in the literature.

between supervised and self-supervised learning. However, this connection has largely been addressed implicitly through experiments and has not been elucidated properly. Therefore, it is difficult to say we have a satisfactory theory linking supervised and self-supervised learning. To explore this connection, we first cast a supervised learning problem as an optimization problem and then extend to formulate a self-supervised learning problem, leveraging natural approximations. Subsequently, we convert the objective function into a more manageable form under certain assumptions. Then, eventually, our problem is reduced to minimizing an upper bound of the objective function.

Our framework provides an explanation of the problem that self-supervised learning solves. We show that the loss induced from our objective function is closely related to the normalized temperature-scaled cross-entropy (NT-Xent) loss in SimCLR (Chen et al., 2020a), which serves as a hub for many algorithms. We introduce the concept of *prototype representation bias*, which arises naturally during the approximation process. It provides insight into a data augmentation strategy. We also introduce a loss inspired by our framework, which we term the *balanced contrastive loss*. We then emphasize the significance of striking the balance between attracting and repelling components of the loss. As a result, our work helps understand self-supervised learning in a more structured and systematic way.

Contributions of our work are summarized as follows:

1. We propose a unified theoretical framework that formalizes self-supervised learning as an approximation of supervised learning, bridging a critical gap in the literature (Section 3).
2. From the theoretical framework, we derive a mathematical foundation for commonly used contrastive losses, particularly InfoNCE-type losses (Section 4).
3. The framework unifies common practices and explains the coexistence of asymmetric and symmetric approaches, enhancing understanding of the field (Section 5).
4. We introduce prototype representation bias and balanced contrastive loss, offering insights into self-supervised learning and the role of balancing parameters (Section 6).

2 Related work

Contrastive losses Our work falls in the category of contrastive learning characterized by contrastive loss. The concept of contrastive loss was introduced in Chopra et al. (2005). From this, several different types of contrastive losses has emerged. The triplet loss simultaneously considers three representations, each serving as an anchor, a positive sample, and a negative sample (Weinberger & Saul, 2009; Chechik et al., 2010). Furthermore, the $(m+1)$-tuplet loss treats $m+1$ representations: an anchor, a positive sample, and $m-1$ negative samples, and it is composed in the form of a softmax function (Sohn, 2016). Wu et al. (2018) combines a temperature parameter and proximal regularization to have the noise-contrastive estimation (NCE) loss. The NT-Xent loss (equivalently, the InfoNCE loss (Oord et al., 2018)) is obtained by constructing a cross-entropy form loss using $2m$ augmented images from a minibatch of m images (Chen et al., 2020a). Wang & Isola (2020) investigates the alignment and uniformity properties of the contrastive loss in an asymptotic setting. In Khosla et al. (2020), the concept of contrastive loss is applied in reverse to the supervised setting. In our work, we lay a foundation for the contrastive losses.

Views on self-supervised learning There have been attempts to express contrastive learning approaches in different languages. There is an approach that provides unified views bridging contrastive learning and covariance-based learning (Huang et al., 2021; Garrido et al., 2022; Lee et al., 2021; Balestriero & LeCun, 2022). There is another approach that interprets contrastive learning as maximizing the mutual information of positive pairs (Hjelm et al., 2018; Oord et al., 2018; Bachman et al., 2019; Wang & Isola, 2020; Li et al., 2021; Aitchison & Ganev, 2024). In addition, there have been attempts to frame self-supervised learning through clustering (Caron et al., 2020), bootstrapping (Grill et al., 2020), semi-supervised learning (Chen et al., 2020b), or knowledge distillation (Caron et al., 2021; Oquab et al., 2023). Previous works provide valuable insights by either revealing specific aspects or bridging different methods. However, while many approaches allude to the idea of supervision, they do not provide an explanation for how attracting or repelling pseudo-labels mathematically translates into attracting or repelling other samples. Our work is to formulate the problem in a principled manner from scratch and systematically outline the step-by-step transition from this formulation to widely used methods.

3 PROBLEM FORMULATION

In this section, we first formulate a supervised representation learning problem as an optimization problem, followed by its self-supervised counterpart. Throughout the paper, we use uppercase letters to denote random elements, lowercase letters to denote non-random elements (including realizations of the random elements), and calligraphic letters to denote sets.

3.1 SUPERVISED REPRESENTATION LEARNING PROBLEM

Let $\mathcal{X} \times \mathcal{Y}$ be a dataset comprising images and their associated visual concepts (represented as labels) of interest. To exploit the dataset to the fullest, we consider a set of transformations $\mathcal{T}$ that preserve the visual concepts and leverage them to create an augmented dataset.[3] Then, we define the augmented dataset induced by $\mathcal{T}$ as

$$\mathcal{T}(\mathcal{X}) \times \mathcal{Y} := \{(t(x), y) : (x, y) \in \mathcal{X} \times \mathcal{Y} \text{ and } t \in \mathcal{T}\}. \tag{1}$$

Equipped with the augmented dataset, we want to train an encoder $f_\theta : \mathcal{X} \to \mathbb{R}^d \setminus \{0\}$ which is parameterized by learnable parameters θ. It maps an image $t(x)$ to its representation $f_\theta(t(x))$. Typically, the representation dimension d is small relative to the image size. By training the encoder, our goal is to make representations of images with the same visual concept, gathered close together, while representations of images with different visual concepts are meaningfully distant from each other. To keep the theoretical framework intuitive and concise, we begin with just these two fundamental ideas: positive samples are clustered, while negative samples are separated.

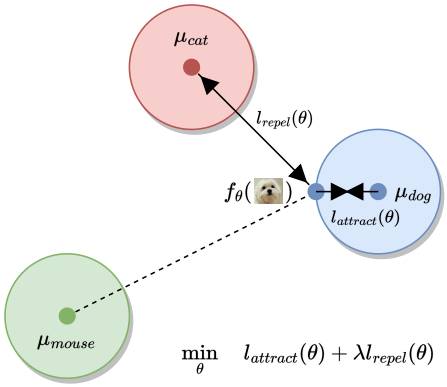

Figure 1: **Supervised learning as an optimization.** $l_{attract}(\theta)$ encourages the image representation to attract the prototype representation μ_{dog} that shares the visual concept of that image. $l_{repel}(\theta)$ prompts the image representation to repel the prototype representation μ_{cat} that is closest among those not sharing the visual concept of that image. The parameter λ balances the two losses.

To achieve our goal, we employ the concept of *prototype representation* of a visual concept to set targets for images (Li et al., 2020; Caron et al., 2020). This denotes a point in the representation space that embodies the visual concept. To see the whole approximation process, we start by assuming that an oracle gives the ideal prototype representation, which can serve as a common target for images with the same visual concept during training. However, since such an oracle does not exist in reality, we later construct the prototype representation using available data.

From now on, we tag a data point $(t(x), y) \in \mathcal{T}(\mathcal{X}) \times \mathcal{Y}$ and base the formulation on it. Let $l_{attract}(\theta)$ be the loss for the image representation $f_\theta(t(x))$ to approach the prototype representation μ_y of its own label, and $l_{repel}(\theta)$ be the loss for the image representation to distance from the prototype representations $\mu_{y'}$ of other labels. Then, we formulate the supervised representation learning problem as the following optimization problem:

$$\min_\theta \quad l_{attract}(\theta) + \lambda l_{repel}(\theta) \tag{2}$$

where $\lambda > 0$ is a parameter which balances the two losses.

In contrastive learning, there is no need to repel negative samples that are already dissimilar enough. In this context, we only repel the prototype representation with the maximum similarity among those

[3] Note that the choice of data augmentation can also be seen as a type of supervision (Xiao et al., 2020). By treating the labels of augmented images as identical, we supervise the resolution at which the model should be transformation invariant. Therefore, unlike $\mathcal{X}$, $\mathcal{T}(\mathcal{X})$ contains partial information about the labels, which enables self-supervised learning.

representing distinct labels. Then, our problem becomes as follows:

$$\min_{\theta} \quad -s\left(f_\theta(t(x)), \mu_y\right) + \lambda \max_{y' \neq y} s\left(f_\theta(t(x)), \mu_{y'}\right) \tag{3}$$

where $s(\cdot, \cdot)$ is a similarity measure. For a better understanding, refer to Figure 1.

Note that our formulation is similar to minimizing the triplet loss in spirit (Chechik et al., 2010; Schroff et al., 2015; Schultz & Joachims, 2003; Arora et al., 2019). In our formulation, we can see $f_\theta(t(x))$ as the anchor, the prototype representation μ_y as the positive sample, and the prototype representation $\mu_{y'}$ as the negative sample. Only considering the negative sample with maximum similarity is related to the concept of hard negative mining (Girshick, 2015; Faghri et al., 2017; Oh Song et al., 2016). This idea has sometimes been implemented through the introduction of the concept of support vectors or margin (Cortes & Vapnik, 1995; Schroff et al., 2015). Pursuing this to the extreme leads us to repel the most challenging example, namely, the negative sample with maximum similarity.

Now, we construct the prototype representations. For a given label y, a natural choice for the prototype representation of the label is the expectation of the representations of the images with the same label, i.e.,

$$\mathbb{E}_{T,X|y} f_\theta(T(X)) \tag{4}$$

where T is distributed over $\mathcal{T}$, and X is conditionally distributed over $\{x : (x, y) \in \mathcal{X} \times \mathcal{Y}\}$. Plugging it to Equation (3), our problem becomes as follows:

$$\min_{\theta} \quad -s\left(f_\theta(t(x)), \mathbb{E}_{T,X|y} f_\theta(T(X))\right) + \lambda \max_{y' \neq y} s\left(f_\theta(t(x)), \mathbb{E}_{T',X'|y'} f_\theta(T'(X'))\right) \tag{5}$$

where T' and X' are independent copies of T and X, respectively.

3.2 Self-supervised representation learning problem

In the self-supervised learning regime, we do not have access to the labels. So, we use a surrogate prototype representation for the image $t(x)$ as the target. We construct it as the expectation of the representations of the *available* images sharing the same label as $t(x)$, i.e.,

$$\mathbb{E}_T f_\theta(T(x)). \tag{6}$$

In Section 5, we demonstrate the importance of finding a data augmentation strategy that approximates well from the prototype representation $\mathbb{E}_{T,X|y} f_\theta(T(X))$ to the surrogate prototype representation $\mathbb{E}_T f_\theta(T(x))$. Plugging it in the attracting component of Equation (5), we rewrite our problem as follows:

$$\min_{\theta} \quad -s\left(f_\theta(t(x)), \mathbb{E}_T f_\theta(T(x))\right) + \lambda \max_{y' \neq y} s\left(f_\theta(t(x)), \mathbb{E}_{T',X'|y'} f_\theta(T'(X'))\right). \tag{7}$$

Note that we leave the repelling component as is since it can be managed without modification. In Section 4, we find an upper bound of the above objective function, and in Section 5, we show the upper bound can be minimized using a Siamese network. Refer to Figure 2 for a better understanding.

4 Theoretical derivation

In this section, we determine upper bounds of the attracting and repelling components. Our objective is to minimize these upper bounds, addressing the optimization problem discussed in the previous section.

4.1 Attracting component

We first find an upper bound for the attracting component by making the following assumptions based on common practice.

Assumption 4.1 (cosine similarity)**.** The similarity measure $s(\cdot, \cdot)$ is cosine similarity, i.e., $s(x_1, x_2) = x_1 \cdot x_2 / (\|x_1\| \|x_2\|)$. When we say $s(x_1, x_2)$, we assume x_1 and x_2 are nonzero.

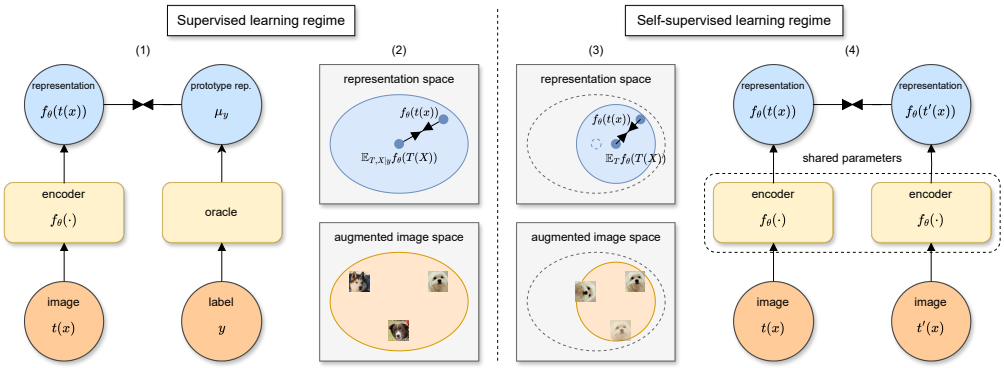

Figure 2: **Self-supervised learning as an approximation of supervised learning.** (1) In an ideal supervised regime, the ideal prototype representation μ_y is given by an oracle. (2) In a realistic supervised regime, the prototype representation is constructed as the expectation $\mathbb{E}_{T,X|y} f_\theta(T(X))$ of the representations of the images with the same label y. (3) In a self-supervised regime, a surrogate prototype representation is constructed as the expectation $\mathbb{E}_T f_\theta(T(x))$ of the representations of the available images sharing the same label as $t(x)$. (4) This can be effectively implemented using a Siamese network.

Assumption 4.2 (l_2-normalization)**.** Representations at the end of the encoder are l_2-normalized so that $\|f_\theta(t(x))\| = 1$, i.e., $f_\theta : \mathcal{X} \to \mathbb{S}^{d-1}$.

We additionally make a technical assumption which means that the two vectors $f_\theta(t(x))$ and $\mathbb{E}_T f_\theta(T(x))$ lie in the same hemisphere. Informally speaking, this means that the augmentation does not distort the image too much, so $\mathbb{E}_T f_\theta(T(x))$ does not point in a completely different direction.

Assumption 4.3 (technical assumption)**.** $f_\theta(t(x)) \cdot \mathbb{E}_T f_\theta(T(x)) \geq 0$.

Theorem 4.4 (upper bound of the attracting component)**.** *Assume Assumption 4.1, 4.2, and 4.3 hold. Then,*

$$-s\left(f_\theta(t(x)), \mathbb{E}_T f_\theta(T(x))\right) \leq -\mathbb{E}_T s\left(f_\theta(t(x)), f_\theta(T(x))\right). \tag{8}$$

Proof. Refer to Appendix A.1.1. □

We approximate the upper bound and obtain the following sample analog:

$$\widetilde{l}_{attract}(\theta) := -\frac{1}{|\hat{\mathcal{T}}|} \sum_{t' \in \hat{\mathcal{T}}} s\left(f_\theta(t(x)), f_\theta(t'(x))\right) \tag{9}$$

where $\hat{\mathcal{T}}$ is the set of transformation samples.

4.2 Repelling Component

We now find an upper bound for the repelling component by making the following assumption.

Assumption 4.5 (balanced dataset)**.** Labels are uniformly distributed, i.e., $p(y) = \frac{1}{n}$, where n is the finite number of labels.

Theorem 4.6 (upper bound of the repelling component)**.** *Assume Assumption 4.1, 4.2, and 4.5 hold. Let* $\nu := \min_{y' \neq y} \|\mathbb{E}_{T',X'|y'} f_\theta(T'(X'))\|$*. Then, for all* $\alpha > 0$*,*

$$\max_{y' \neq y} s\left(f_\theta(t(x)), \mathbb{E}_{T',X'|y'} f_\theta(T'(X'))\right) \leq \mathbb{E}_{T'}\left[\frac{1}{\nu\alpha} \log \mathbb{E}_{X'} \exp\left(\alpha s\left(f_\theta(t(x)), f_\theta(T'(X'))\right)\right)\right] + \frac{1}{\nu\alpha} \log n. \tag{10}$$

Proof. We approximate the maximum function by the log-sum-exp function and apply Jensen inequality to pull out the expectations. For the detailed proof, refer to Appendix A.1.2. □

If we approximate the upper bound and trim the constant terms, which are not relevant to optimization, we obtain the following:

$$\widetilde{l}_{repel}(\theta) := \frac{1}{|\hat{\mathcal{T}}|} \sum_{t' \in \hat{\mathcal{T}}} \frac{1}{\nu\alpha} \log \sum_{x' \in \hat{\mathcal{X}}} \exp(\alpha s(f_\theta(t(x)), f_\theta(t'(x')))) \tag{11}$$

where $\hat{\mathcal{T}}$ is the set of transformation samples, and $\hat{\mathcal{X}}$ is the set of image samples.

4.3 Total loss

By combining Equation (9) and (11), the total loss $\widetilde{l}(\theta) := \widetilde{l}_{attract}(\theta) + \lambda \widetilde{l}_{repel}(\theta)$ is as follows:

$$\widetilde{l}(\theta) = \frac{1}{|\hat{\mathcal{T}}|} \sum_{t' \in \hat{\mathcal{T}}} \left[-s\left(f_\theta(t(x)), f_\theta(t'(x))\right) + \frac{\lambda}{\nu} \left[\frac{1}{\alpha} \log \sum_{x' \in \hat{\mathcal{X}}} \exp(\alpha s(f_\theta(t(x)), f_\theta(t'(x')))) \right] \right]. \tag{12}$$

By rearranging, we have

$$\widetilde{l}(\theta) = \frac{1}{\alpha|\hat{\mathcal{T}}|} \sum_{t' \in \hat{\mathcal{T}}} \left[-\log \frac{\exp(\alpha s\left(f_\theta(t(x)), f_\theta(t'(x))\right))}{\left(\sum_{x' \in \hat{\mathcal{X}}} \exp(\alpha s(f_\theta(t(x)), f_\theta(t'(x'))))\right)^{\lambda/\nu}} \right]. \tag{13}$$

Note that this equation and the NT-Xent in SimCLR are similar in their forms, which we discuss in more detail in the next section.

5 Understanding self-supervised learning

In this section, we discuss components of self-supervised learning algorithms within our framework, focusing on SimCLR (Chen et al., 2020a), which has served as a central point for many algorithms.

In experiments in this section, we utilize SimCLR with a temperature parameter τ of 0.5, employing ImageNet (Deng et al., 2009) as the dataset and ResNet-50 (He et al., 2016) as the backbone. We assess top-1 accuracy using linear evaluation, a standard protocol for evaluating self-supervised learning algorithms. Note that, since ImageNet contains 1,000 classes, the chance-level accuracy is 0.1%. For a fair comparison, all settings are kept the same except for the specific factor under investigation. For the detailed implementation, refer to A.3.

5.1 Architecture: Siamese networks

When approximating the upper bound $-\mathbb{E}_T s\left(f_\theta(t(x)), f_\theta(T(x))\right)$ in Equation (8), we compare the similarity between two representations $f_\theta(t(x))$ and $f_\theta(t'(x))$. This is suitable for implementation by a Siamese network (Bromley et al., 1993), which consists of two encoders. We augment a single image x to obtain two differently augmented $t(x)$ and $t'(x)$. Then, we pass them through the two encoders f_θ that share the parameter θ and compare the similarity of the outputs. So, our derivation shows that considering similarity with the prototype representation aligns well with using a Siamese network, which is a common architecture in self-supervised learning.

Siamese networks are fundamentally symmetric in that the two encoders often have the same architecture and share parameters. However, there are algorithms aimed at enhancing performance by introducing asymmetry into Siamese networks (He et al., 2020; Chen & He, 2021; Grill et al., 2020; Caron et al., 2020; 2021; Oquab et al., 2023; Tian et al., 2021). In such cases, it is empirically shown to be helpful to ensure that the variance of the outputs from one encoder is lower than that from the other encoder (Wang et al., 2022). The encoder with the lower variance is referred to as the target or teacher encoder, and the encoder with the higher variance is referred to as the source or student encoder. In our problem formulation, the original attracting component in Equation (8) is $-s\left(f_\theta(t(x)), \mathbb{E}_T f_\theta(T(x))\right)$ where the two attracting objects $f_\theta(t(x))$ and $\mathbb{E}_T f_\theta(T(x))$ are asymmetric. Note that $\mathbb{E}_T f_\theta(T(x))$

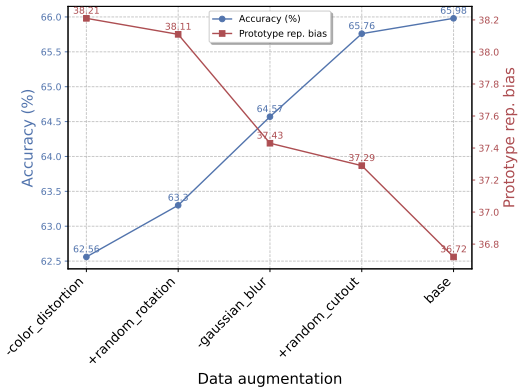

Figure 3: **Accuracy vs. prototype representation bias.** We investigate the relationship between accuracy and prototype representation bias by adding or removing transformations from SimCLR's data augmentation strategy (base). Lower prototype representation bias tends to result in higher accuracy.

can be approximated by $\frac{1}{n}\sum_{i=1}^{n} f_\theta(T_i(x))$, and $\frac{1}{n}\sum_{i=1}^{n} f_\theta(T_i(x))$ has less variance than $f_\theta(T(x))$. So, our problem formulation and Theorem 4.4 may provide insight to understand why there exist both symmetry and asymmetry themes in the self-supervised learning literature.

5.2 Loss: NT-Xent

Let $\{x_1, \ldots, x_m\}$ be a minibatch of m images. If we transform each image in two different ways and pass them through the encoder, we obtain representation pairs $\{(f_\theta(t(x_i)), f_\theta(t'(x_i))) : i = 1, \ldots, m\}$ of $2m$ augmented images, which we denote as $\{(z_i, z_i') : i = 1, \ldots, m\}$. Then, in the case of $\lambda = \nu$, the summand in Equation (13) can be implemented as

$$-\log \frac{\exp(\alpha s(z_i, z_i'))}{\sum_{j\in[m]\setminus\{i\}} \exp(\alpha s(z_i, z_j'))} \tag{14}$$

where $[m] := \{1, \ldots, m\}$.

On the other hand, in the NT-Xent loss used in SimCLR, if we let the temperature parameter τ be $1/\alpha$, the NT-Xent loss is represented as

$$-\log \frac{\exp(\alpha s(z_i, z_i'))}{\sum_{j\in[m]} \exp(\alpha s(z_i, z_j')) + \sum_{j\in[m]\setminus\{i\}} \exp(\alpha s(z_i, z_j))}. \tag{15}$$

This is a variant of Equation (14). Having the second summation in the denominator can be seen as a method to fully exploit the provided representations, since (z_i, z_j) are also negative pairs when $j \neq i$. When considering the first summation in the denominator, Yeh et al. (2022) empirically demonstrated that it performs better when the sum is over $[m] \setminus \{i\}$ as in Equation (14) rather than $[m]$. Expressions such as cross-entropy and temperature frame contrastive losses in the form of the Boltzmann (or Gibbs) distribution. Our framework offers another perspective on the losses.

5.3 Data augmentation: debiased prototype representation

When transitioning from supervised learning to self-supervised learning, we approximate the prototype representation $\mathbb{E}_{T,X|y} f_\theta(T(X))$ with the surrogate prototype representation $\mathbb{E}_T f_\theta(T(x))$. Therefore, we investigate whether accuracy increases as the two become closer. For this purpose, we define the *prototype representation bias* as follows

$$\mathbb{E}_{(X_0,Y_0)} \|\mathbb{E}_{T,X|Y_0} f_\theta(T(X)) - \mathbb{E}_T f_\theta(T(X_0))\|. \tag{16}$$

We then compare the values by changing the distribution of T through data augmentation. We compare SimCLR's default data augmentation (`base`) with cases where we exclude Gaussian

blur (`-gaussian_blur`) and color distortion (`-color_distortion`), and with cases where we include random cutout (`+random_cutout`) and random rotation (`+random_rotation`), resulting in a total of five scenarios.

Figure 3 shows that using data augmentation with debiased prototype representation leads to an increase in accuracy. It also shows the default data augmentation of SimCLR achieves the highest accuracy while exhibiting the smallest prototype representation bias. Despite the expectation that enriching data augmentation by adding transformations would be beneficial for training, the accuracy still decreases. This may be because the added transformations exacerbate the prototype representation bias.

5.4 Similarity measure: cosine similarity with normalization

When computing similarity between two representations, many self-supervised learning algorithms including SimCLR normalize the representations and calculate cosine similarity as in Assumption 4.1 and 4.2. To empirically show the significance of these assumptions, we compare three cases: 1) cosine similarity with normalization, 2) dot product without normalization, and 3) negative Euclidean distance without normalization.[4] Table 1 shows that normalization is crucial. Without normalization, the accuracy in the case of negative Euclidean distance is higher than that of dot product. This may be because Euclidean distance measures spatial dissimilarity in a more straightforward manner.

Table 1: Similarity measure. The performance is better for the case of cosine similarity with normalization.

Similarity measure		
CS w/ l_2	Dot w/o l_2	-Eucl. w/o l_2
65.98	0.43	10.63

5.5 Dataset: balanced

There are some results that contrastive learning algorithms perform better on balanced datasets, where labels are uniformly distributed (Assran et al., 2022b;a; Zhou et al., 2022) as in Assumption 4.5. Refer to Subsection A.4.4 for experiments in our setting.

6 Empirical study

In this section, we introduce a loss that is inspired from the form of Equation (12). To reduce clutter, we rewrite λ/ν as λ. For one representation z in $2m$ representations generated from a minibatch of m images, we define our loss for the representation as follows:

$$-s(z, z^+) + \lambda \left[\frac{1}{\alpha} \log \sum_{z^-} \exp(\alpha s(z, z^-)) \right] \tag{17}$$

where (z, z^+) is the positive pair and (z, z^-) are $2(m-1)$ negative pairs. The cost for the whole minibatch is then calculated by taking the mean of the losses of all representations. Note that the attracting component consists of one attracting force, and the repelling component consists of multiple repelling forces. We term the loss the *balanced contrastive loss*.

There are two hyperparameters $\alpha > 0$ and $\lambda > 0$ in the balanced contrastive loss. We refer to these as the *balancing parameters* since each is in charge of two different types of balancing in contrastive learning. The parameter $\alpha > 0$ adjusts the relative magnitudes within the repelling forces. Note that the repelling component is a smooth approximation to the maximum function (refer to Lemma A.1 and Wang & Liu (2021)):

$$\lim_{\alpha \to \infty} \left[\frac{1}{\alpha} \log \sum_{z^-} \exp(\alpha s(z, z^-)) \right] = \max_{z^-} s(z, z^-). \tag{18}$$

[4]Note that when dealing with two normalized vectors, cosine similarity is equivalent to the dot product. Additionally, negative Euclidean distance with normalization is equivalent to cosine similarity with normalization since $-\|a-b\|^2 = -2 + 2a \cdot b$.

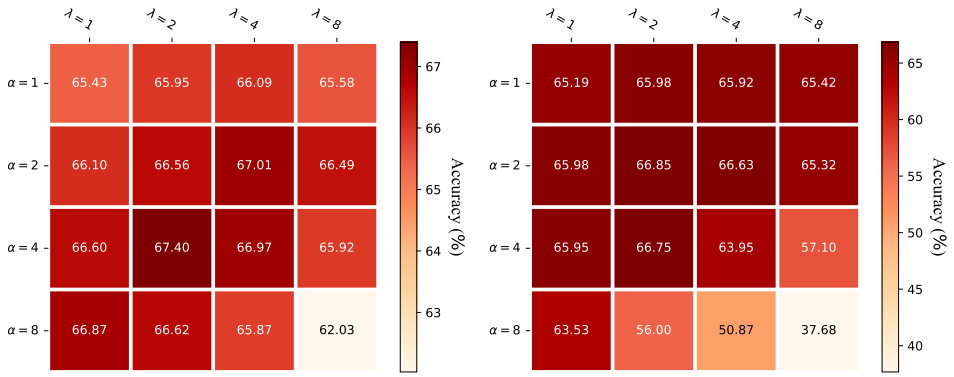

(a) Balanced contrastive loss

(b) Generalized NT-Xent loss

Figure 4: **Impact of balancing parameters α and λ.** Better balancing can be accomplished through the adjustments of the balancing parameters.

If α is large, the repelling forces with representations having high similarities contribute more in the overall repelling component. In self-supervised learning, negative samples may have images with the same label (called sampling bias in Chuang et al. (2020)). So, if we make α too large, there is a risk of repelling images with the same label. Therefore, setting the value of α appropriately can be thought of as hedging the risk with multiple negative samples. This also offers insight into the role of the temperature parameters of InfoNCE-type losses. On the other hand, the parameter $\lambda > 0$ adjusts the relative magnitudes of the attracting and repelling forces.

To study the impact of balancing parameters α and λ, we test our loss over a grid of parameters $\{(\alpha, \lambda) : \alpha, \lambda \in \{1, 2, 4, 8\}\}$. We also investigate the case where the positive pair is included in the summation in Equation (17). We call the case the generalized NT-Xent loss here since it is equivalent to the NT-Xent loss when $\lambda = 1$. Figure 4 illustrates the changes in accuracy based on various combinations of the parameters. The balanced contrastive loss generally achieves higher maximum accuracies than the generalized NT-Xent loss in this experiment.

For the balanced contrastive loss, the highest accuracy is achieved when $(\alpha, \lambda) = (4, 2)$, and for the generalized NT-Xent loss, the highest accuracy is achieved when $(\alpha, \lambda) = (2, 2)$. In both cases, the highest accuracy is not achieved when $\lambda = 1$. This highlights the significance of the balancing parameter λ. Additionally in both scenarios, it is crucial for α to have an appropriate value that is not too large or too small. Specifically for the generalized NT-Xent, it is advantageous to set α to a smaller value compared to the balanced contrastive loss. This may be due to the presence of the positive sample in the repelling component, meaning that increasing α results in a larger repulsion of the positive sample. Given that the chance-level accuracy for ImageNet is 0.1, this performance difference is notable, achieved solely through weight adjustments. The results also suggest that the current forms of contrastive losses may be limited.

7 Discussion

The potential connection between supervised and self-supervised learning has been implied in practical algorithms. It has been interpreted from perspectives such as bootstrapping, clustering, and knowledge distillation, which can align with our framework. From the bootstrapping perspective (Grill et al., 2020), the idea is to construct targets solely based on the representations without any external input. This aligns with the framework, where prototype representations are built solely from the representations themselves and used as pseudo-labels. In this line of work, a predictor is often employed, which can be seen as an additional module designed to match the pseudo-labels (Chen & He, 2021). From the clustering perspective (Tian et al., 2017; Caron et al., 2020), the goal is to ensure consistency in the cluster assignments of transformed images. This aligns with the framework in that the representations of transformed images converge toward a single prototype representation, guiding them to belong to the same cluster. From the knowledge distillation perspective (Xu et al., 2020; Caron et al., 2021), self-supervised learning involves a teacher network transferring knowledge

to a student network. This aligns with the framework in that the output of one encoder serves as a prototype representation, guiding the output of the other encoder to match it in the formula we ultimately want to optimize.

8 Conclusion

In this work, a self-supervised representation learning problem is theoretically conceptualized as an approximation of a supervised representation learning problem. We first formulate the supervised learning problem concisely and then investigate how its natural approximation arises in the absence of labels. We break down the process into individual steps, allowing the community to focus on improving each step. Our framework enhances an understanding of existing algorithms. The loss derived at the end is related to widely used InfoNCE-type losses. Additionally, our framework provides insights into the biases of prototype representations and balancing in contrastive loss, which can be considered when designing an optimal algorithm. It also provides richer context for components of existing algorithms, such as data augmentation, temperature hyperparameters, and symmetric/asymmetric architecture. Our work aims to contribute to building a firm foundation for self-supervised learning. We hope that our work will benefit the self-supervised learning community by serving as a basis and providing guidance for research.

Reproducibility Statement

We have made every effort to ensure the reproducibility of our work. The following resources and materials are provided to help reproduce our results:

- The proofs of all theoretical results, along with explanations of any assumptions made, are included in the appendix (refer to Subsection A.1).
- The source code for the experiments, along with instructions for running the code, is included as supplementary material and will be made publicly available upon publication (refer to the attached `.zip` file).
- Implementation details including datasets, pre-processing steps, model configurations, hyperparameters, evaluation metrics are specified in the main paper and further elaborated in the appendix (refer to Section 5 and Subsection A.3).

We believe these resources and materials will facilitate the research community to reproduce our results.

References

Laurence Aitchison and Stoil Krasimirov Ganev. InfoNCE is variational inference in a recognition parameterised model. *Transactions on Machine Learning Research*, 2024. ISSN 2835-8856. URL https://openreview.net/forum?id=chbRsWwjax.

Sanjeev Arora, Hrishikesh Khandeparkar, Mikhail Khodak, Orestis Plevrakis, and Nikunj Saunshi. A theoretical analysis of contrastive unsupervised representation learning. *arXiv preprint arXiv:1902.09229*, 2019.

Mahmoud Assran, Mathilde Caron, Ishan Misra, Piotr Bojanowski, Florian Bordes, Pascal Vincent, Armand Joulin, Mike Rabbat, and Nicolas Ballas. Masked siamese networks for label-efficient learning. In *European Conference on Computer Vision*, pp. 456–473. Springer, 2022a.

Mido Assran, Randall Balestriero, Quentin Duval, Florian Bordes, Ishan Misra, Piotr Bojanowski, Pascal Vincent, Michael Rabbat, and Nicolas Ballas. The hidden uniform cluster prior in self-supervised learning. In *The Eleventh International Conference on Learning Representations*, 2022b.

Philip Bachman, R Devon Hjelm, and William Buchwalter. Learning representations by maximizing mutual information across views. *Advances in neural information processing systems*, 32, 2019.

Randall Balestriero and Yann LeCun. Contrastive and non-contrastive self-supervised learning recover global and local spectral embedding methods. *Advances in Neural Information Processing Systems*, 35:26671–26685, 2022.

Randall Balestriero, Mark Ibrahim, Vlad Sobal, Ari Morcos, Shashank Shekhar, Tom Goldstein, Florian Bordes, Adrien Bardes, Gregoire Mialon, Yuandong Tian, et al. A cookbook of self-supervised learning. *arXiv preprint arXiv:2304.12210*, 2023.

Lucas Beyer, Olivier J Hénaff, Alexander Kolesnikov, Xiaohua Zhai, and Aäron van den Oord. Are we done with imagenet? *arXiv preprint arXiv:2006.07159*, 2020.

Stephen P Boyd and Lieven Vandenberghe. *Convex optimization*. Cambridge university press, 2004.

Jane Bromley, Isabelle Guyon, Yann LeCun, Eduard Säckinger, and Roopak Shah. Signature verification using a" siamese" time delay neural network. *Advances in neural information processing systems*, 6, 1993.

Mathilde Caron, Ishan Misra, Julien Mairal, Priya Goyal, Piotr Bojanowski, and Armand Joulin. Unsupervised learning of visual features by contrasting cluster assignments. *Advances in neural information processing systems*, 33:9912–9924, 2020.

Mathilde Caron, Hugo Touvron, Ishan Misra, Hervé Jégou, Julien Mairal, Piotr Bojanowski, and Armand Joulin. Emerging properties in self-supervised vision transformers. In *Proceedings of the IEEE/CVF international conference on computer vision*, pp. 9650–9660, 2021.

Gal Chechik, Varun Sharma, Uri Shalit, and Samy Bengio. Large scale online learning of image similarity through ranking. *Journal of Machine Learning Research*, 11(3), 2010.

Ting Chen, Simon Kornblith, Mohammad Norouzi, and Geoffrey Hinton. A simple framework for contrastive learning of visual representations. In *International conference on machine learning*, pp. 1597–1607. PMLR, 2020a.

Ting Chen, Simon Kornblith, Kevin Swersky, Mohammad Norouzi, and Geoffrey E Hinton. Big self-supervised models are strong semi-supervised learners. *Advances in neural information processing systems*, 33:22243–22255, 2020b.

Xinlei Chen and Kaiming He. Exploring simple siamese representation learning. In *Proceedings of the IEEE/CVF conference on computer vision and pattern recognition*, pp. 15750–15758, 2021.

Sumit Chopra, Raia Hadsell, and Yann LeCun. Learning a similarity metric discriminatively, with application to face verification. In *2005 IEEE computer society conference on computer vision and pattern recognition (CVPR'05)*, volume 1, pp. 539–546. IEEE, 2005.

Ching-Yao Chuang, Joshua Robinson, Yen-Chen Lin, Antonio Torralba, and Stefanie Jegelka. Debiased contrastive learning. *Advances in neural information processing systems*, 33:8765–8775, 2020.

Corinna Cortes and Vladimir Vapnik. Support-vector networks. *Machine learning*, 20:273–297, 1995.

Jia Deng, Wei Dong, Richard Socher, Li-Jia Li, Kai Li, and Li Fei-Fei. Imagenet: A large-scale hierarchical image database. In *2009 IEEE conference on computer vision and pattern recognition*, pp. 248–255. Ieee, 2009.

Carl Doersch, Abhinav Gupta, and Alexei A Efros. Unsupervised visual representation learning by context prediction. In *Proceedings of the IEEE international conference on computer vision*, pp. 1422–1430, 2015.

Fartash Faghri, David J Fleet, Jamie Ryan Kiros, and S Vse+ Fidler. Improving visual-semantic embeddings with hard negatives. *arXiv preprint arXiv:1707.05612*, pp. 7161–7170, 2017.

Quentin Garrido, Yubei Chen, Adrien Bardes, Laurent Najman, and Yann Lecun. On the duality between contrastive and non-contrastive self-supervised learning. *arXiv preprint arXiv:2206.02574*, 2022.

LE Ghaoui. Hyper-textbook: Optimization models and applications, 2014.

Spyros Gidaris, Praveer Singh, and Nikos Komodakis. Unsupervised representation learning by predicting image rotations. *arXiv preprint arXiv:1803.07728*, 2018.

Ross Girshick. Fast r-cnn. In *Proceedings of the IEEE international conference on computer vision*, pp. 1440–1448, 2015.

Jean-Bastien Grill, Florian Strub, Florent Altché, Corentin Tallec, Pierre Richemond, Elena Buchatskaya, Carl Doersch, Bernardo Avila Pires, Zhaohan Guo, Mohammad Gheshlaghi Azar, et al. Bootstrap your own latent-a new approach to self-supervised learning. *Advances in neural information processing systems*, 33:21271–21284, 2020.

Jie Gui, Tuo Chen, Jing Zhang, Qiong Cao, Zhenan Sun, Hao Luo, and Dacheng Tao. A survey on self-supervised learning: Algorithms, applications, and future trends, 2023.

Kaiming He, Xiangyu Zhang, Shaoqing Ren, and Jian Sun. Deep residual learning for image recognition. In *Proceedings of the IEEE conference on computer vision and pattern recognition*, pp. 770–778, 2016.

Kaiming He, Haoqi Fan, Yuxin Wu, Saining Xie, and Ross Girshick. Momentum contrast for unsupervised visual representation learning. In *Proceedings of the IEEE/CVF conference on computer vision and pattern recognition*, pp. 9729–9738, 2020.

R Devon Hjelm, Alex Fedorov, Samuel Lavoie-Marchildon, Karan Grewal, Phil Bachman, Adam Trischler, and Yoshua Bengio. Learning deep representations by mutual information estimation and maximization. *arXiv preprint arXiv:1808.06670*, 2018.

Weiran Huang, Mingyang Yi, Xuyang Zhao, and Zihao Jiang. Towards the generalization of contrastive self-supervised learning. *arXiv preprint arXiv:2111.00743*, 2021.

Sergey Ioffe and Christian Szegedy. Batch normalization: Accelerating deep network training by reducing internal covariate shift. In *International conference on machine learning*, pp. 448–456. pmlr, 2015.

Prannay Khosla, Piotr Teterwak, Chen Wang, Aaron Sarna, Yonglong Tian, Phillip Isola, Aaron Maschinot, Ce Liu, and Dilip Krishnan. Supervised contrastive learning. *Advances in neural information processing systems*, 33:18661–18673, 2020.

Alex Krizhevsky, Geoffrey Hinton, et al. Learning multiple layers of features from tiny images.(2009), 2009.

Jason D Lee, Qi Lei, Nikunj Saunshi, and Jiacheng Zhuo. Predicting what you already know helps: Provable self-supervised learning. *Advances in Neural Information Processing Systems*, 34: 309–323, 2021.

Junnan Li, Pan Zhou, Caiming Xiong, and Steven CH Hoi. Prototypical contrastive learning of unsupervised representations. *arXiv preprint arXiv:2005.04966*, 2020.

Yazhe Li, Roman Pogodin, Danica J Sutherland, and Arthur Gretton. Self-supervised learning with kernel dependence maximization. *Advances in Neural Information Processing Systems*, 34: 15543–15556, 2021.

Ilya Loshchilov and Frank Hutter. Sgdr: Stochastic gradient descent with warm restarts. *arXiv preprint arXiv:1608.03983*, 2016.

Mehdi Noroozi and Paolo Favaro. Unsupervised learning of visual representations by solving jigsaw puzzles. In *European conference on computer vision*, pp. 69–84. Springer, 2016.

Hyun Oh Song, Yu Xiang, Stefanie Jegelka, and Silvio Savarese. Deep metric learning via lifted structured feature embedding. In *Proceedings of the IEEE conference on computer vision and pattern recognition*, pp. 4004–4012, 2016.

Aaron van den Oord, Yazhe Li, and Oriol Vinyals. Representation learning with contrastive predictive coding. *arXiv preprint arXiv:1807.03748*, 2018.

Maxime Oquab, Timothée Darcet, Théo Moutakanni, Huy Vo, Marc Szafraniec, Vasil Khalidov, Pierre Fernandez, Daniel Haziza, Francisco Massa, Alaaeldin El-Nouby, et al. Dinov2: Learning robust visual features without supervision. *arXiv preprint arXiv:2304.07193*, 2023.

Emin Orhan, Vaibhav Gupta, and Brenden M Lake. Self-supervised learning through the eyes of a child. *Advances in Neural Information Processing Systems*, 33:9960–9971, 2020.

Utku Ozbulak, Hyun Jung Lee, Beril Boga, Esla Timothy Anzaku, Homin Park, Arnout Van Messem, Wesley De Neve, and Joris Vankerschaver. Know your self-supervised learning: A survey on image-based generative and discriminative training. *arXiv preprint arXiv:2305.13689*, 2023.

Senthil Purushwalkam and Abhinav Gupta. Demystifying contrastive self-supervised learning: Invariances, augmentations and dataset biases. *Advances in Neural Information Processing Systems*, 33:3407–3418, 2020.

Neil Savage. Marriage of mind and machine. *Nature*, 571(7766):S15–S17, 2019.

Madeline C Schiappa, Yogesh S Rawat, and Mubarak Shah. Self-supervised learning for videos: A survey. *ACM Computing Surveys*, 55(13s):1–37, 2023.

Florian Schroff, Dmitry Kalenichenko, and James Philbin. Facenet: A unified embedding for face recognition and clustering. In *Proceedings of the IEEE conference on computer vision and pattern recognition*, pp. 815–823, 2015.

Matthew Schultz and Thorsten Joachims. Learning a distance metric from relative comparisons. *Advances in neural information processing systems*, 16, 2003.

Vaishaal Shankar, Rebecca Roelofs, Horia Mania, Alex Fang, Benjamin Recht, and Ludwig Schmidt. Evaluating machine accuracy on imagenet. In *International Conference on Machine Learning*, pp. 8634–8644. PMLR, 2020.

Kihyuk Sohn. Improved deep metric learning with multi-class n-pair loss objective. *Advances in neural information processing systems*, 29, 2016.

Antti Tarvainen and Harri Valpola. Mean teachers are better role models: Weight-averaged consistency targets improve semi-supervised deep learning results. *Advances in neural information processing systems*, 30, 2017.

Kai Tian, Shuigeng Zhou, and Jihong Guan. Deepcluster: A general clustering framework based on deep learning. In *Machine Learning and Knowledge Discovery in Databases: European Conference, ECML PKDD 2017, Skopje, Macedonia, September 18–22, 2017, Proceedings, Part II 17*, pp. 809–825. Springer, 2017.

Yuandong Tian, Xinlei Chen, and Surya Ganguli. Understanding self-supervised learning dynamics without contrastive pairs. In *International Conference on Machine Learning*, pp. 10268–10278. PMLR, 2021.

Vijay Vasudevan, Benjamin Caine, Raphael Gontijo Lopes, Sara Fridovich-Keil, and Rebecca Roelofs. When does dough become a bagel? analyzing the remaining mistakes on imagenet. *Advances in Neural Information Processing Systems*, 35:6720–6734, 2022.

Feng Wang and Huaping Liu. Understanding the behaviour of contrastive loss. In *Proceedings of the IEEE/CVF conference on computer vision and pattern recognition*, pp. 2495–2504, 2021.

Tongzhou Wang and Phillip Isola. Understanding contrastive representation learning through alignment and uniformity on the hypersphere. In *International conference on machine learning*, pp. 9929–9939. PMLR, 2020.

Xiao Wang, Haoqi Fan, Yuandong Tian, Daisuke Kihara, and Xinlei Chen. On the importance of asymmetry for siamese representation learning. In *Proceedings of the IEEE/CVF conference on computer vision and pattern recognition*, pp. 16570–16579, 2022.

Kilian Q Weinberger and Lawrence K Saul. Distance metric learning for large margin nearest neighbor classification. *Journal of machine learning research*, 10(2), 2009.

Zhirong Wu, Yuanjun Xiong, Stella X Yu, and Dahua Lin. Unsupervised feature learning via non-parametric instance discrimination. In *Proceedings of the IEEE conference on computer vision and pattern recognition*, pp. 3733–3742, 2018.

Tete Xiao, Xiaolong Wang, Alexei A Efros, and Trevor Darrell. What should not be contrastive in contrastive learning. *arXiv preprint arXiv:2008.05659*, 2020.

Guodong Xu, Ziwei Liu, Xiaoxiao Li, and Chen Change Loy. Knowledge distillation meets self-supervision. In *European conference on computer vision*, pp. 588–604. Springer, 2020.

Chun-Hsiao Yeh, Cheng-Yao Hong, Yen-Chi Hsu, Tyng-Luh Liu, Yubei Chen, and Yann LeCun. Decoupled contrastive learning. In *European conference on computer vision*, pp. 668–684. Springer, 2022.

Yang You, Igor Gitman, and Boris Ginsburg. Large batch training of convolutional networks. *arXiv preprint arXiv:1708.03888*, 2017.

Richard Zhang, Phillip Isola, and Alexei A Efros. Colorful image colorization. In *European conference on computer vision*, pp. 649–666. Springer, 2016.

Zhihan Zhou, Jiangchao Yao, Yan-Feng Wang, Bo Han, and Ya Zhang. Contrastive learning with boosted memorization. In *International Conference on Machine Learning*, pp. 27367–27377. PMLR, 2022.

A APPENDIX

A.1 PROOFS

This subsection presents the proofs of Theorem 4.4 and Theorem 4.6.

A.1.1 PROOF OF THEOREM 4.4

We restate the assumptions and the theorem and provide the proof below.

Assumption 4.1 (cosine similarity)**.** The similarity measure $s(\cdot,\cdot)$ is cosine similarity, i.e., $s(x_1, x_2) = x_1 \cdot x_2/(\|x_1\|\|x_2\|)$. When we say $s(x_1, x_2)$, we assume x_1 and x_2 are nonzero.

Assumption 4.2 (l_2-normalization)**.** Representations at the end of the encoder are l_2-normalized so that $\|f_\theta(t(x))\| = 1$, i.e., $f_\theta : \mathcal{X} \to \mathbb{S}^{d-1}$.

Assumption 4.3 (technical assumption)**.** $f_\theta(t(x)) \cdot \mathbb{E}_T f_\theta(T(x)) \geq 0$.

Theorem 4.4 (upper bound of the attracting component)**.** *Assume Assumption 4.1, 4.2, and 4.3 hold. Then,*

$$-s\left(f_\theta(t(x)), \mathbb{E}_T f_\theta(T(x))\right) \leq -\mathbb{E}_T s\left(f_\theta(t(x)), f_\theta(T(x))\right). \tag{8}$$

Proof.

$$-s\left(f_\theta(t(x)), \mathbb{E}_T f_\theta(T(x))\right) \overset{(i)}{=} -\frac{f_\theta(t(x)) \cdot \mathbb{E}_T f_\theta(T(x))}{\|f_\theta(t(x))\|\|\mathbb{E}_T f_\theta(T(x))\|} \tag{19}$$

$$\overset{(ii)}{=} -\frac{f_\theta(t(x)) \cdot \mathbb{E}_T f_\theta(T(x))}{\|\mathbb{E}_T f_\theta(T(x))\|} \tag{20}$$

$$\overset{(iii)}{\leq} -\frac{f_\theta(t(x)) \cdot \mathbb{E}_T f_\theta(T(x))}{\mathbb{E}_T \|f_\theta(T(x))\|} \tag{21}$$

$$\overset{(iv)}{=} -f_\theta(t(x)) \cdot \mathbb{E}_T f_\theta(T(x)) \tag{22}$$

$$\overset{(v)}{=} -\mathbb{E}_T\left[f_\theta(t(x)) \cdot f_\theta(T(x))\right] \tag{23}$$

$$\overset{(vi)}{=} -\mathbb{E}_T\left[\frac{f_\theta(t(x)) \cdot f_\theta(T(x))}{\|f_\theta(t(x))\|\|f_\theta(T(x))\|}\right] \tag{24}$$

$$\overset{(vii)}{=} -\mathbb{E}_T s\left(f_\theta(t(x)), f_\theta(T(x))\right) \tag{25}$$

where (i) and (vii) are by Assumption 4.1, (ii), (iv), and (vi) are by Assumption 4.2, (iii) is by Assumption 4.3, the convexity of l^2-norm (Boyd & Vandenberghe, 2004), and Jensen's inequality, and (v) is by the linearity of expectation. This completes the proof of Theorem 4.4. □

A.1.2 PROOF OF THEOREM 4.6

Before we prove Theorem 4.6, we need three additional lemmas. While the proofs of the lemmas are straightforward, they are not readily available in the existing literature. Therefore, we provide them here for the sake of self-containedness.

Lemma A.1. *For $\alpha > 0$ and $x_i \in \mathbb{R}$, $i = 1, 2, \ldots, n$,*

$$\max_{i=1,\ldots,n} x_i \leq (1/\alpha) \log \sum_{i=1}^{n} \exp(\alpha x_i) \leq \max_{i=1,\ldots,n} x_i + \frac{\log n}{\alpha}, \tag{26}$$

where the equalities hold when α goes to infinity.

Proof. We have

$$\exp\left(\max_{i=1,\ldots,n}(\alpha x_i)\right) \leq \sum_{i=1}^{n} \exp\left(\alpha x_i\right) \leq n \exp\left(\max_{i=1,\ldots,n}(\alpha x_i)\right). \tag{27}$$

Since $\alpha > 0$,

$$\alpha \max_{i=1,\dots,n} x_i \leq \log \sum_{i=1}^{n} \exp(\alpha x_i) \leq \alpha \max_{i=1,\dots,n} x_i + \log n. \tag{28}$$

This completes the proof of Lemma A.1. □

Lemma A.2. *For $\alpha > 0$ and $x_i \in \mathbb{R}$, $i = 1, 2, \dots, n$,*

$$u(x_1, \dots, x_n) := (1/\alpha) \log \sum_{i=1}^{n} \exp(\alpha x_i) \tag{29}$$

is convex on $\mathbb{R}^n$.

Proof. Note that the log-sum-exp function $v(x_1, \dots, x_n) := \log \sum_{i=1}^{n} \exp(x_i)$ is convex on $\mathbb{R}^n$ (Boyd & Vandenberghe, 2004; Ghaoui, 2014). $u(x_1, \dots, x_n) = (1/\alpha)v(\alpha(x_1, \dots, x_n))$, and composition with an affine mapping preserves convexity (Boyd & Vandenberghe, 2004). Thus, $u(x_1, \dots, x_n)$ is also convex on $\mathbb{R}^n$. This completes the proof of Lemma A.2. □

Lemma A.3. *If $g_1(x) \geq 0$ for all x, and $g_2(x) \geq 0$ for some x, then*

$$\max[g_1(x)g_2(x)] \leq \max[g_1(x)] \max[g_2(x)]. \tag{30}$$

Proof. By default, $g_2(x) \leq \max[g_2(x)]$. Since $g_1(x) \geq 0$ for all x, $g_1(x)g_2(x) \leq g_1(x) \max[g_2(x)]$. Taking the maximum of both sides, we have $\max[g_1(x)g_2(x)] \leq \max[g_1(x) \max[g_2(x)]]$. Since $g_2(x) \geq 0$ for some x, $\max[g_2(x)] \geq 0$, and thus $\max[g_1(x)g_2(x)] \leq \max[g_1(x)] \max[g_2(x)]$. This completes the proof of Lemma A.3. □

Now, we are ready to prove Theorem 4.6. We restate the assumption and the theorem and provide the proof below.

Assumption 4.5 (balanced dataset)**.** Labels are uniformly distributed, i.e., $p(y) = \frac{1}{n}$, where n is the finite number of labels.

Theorem 4.6 (upper bound of the repelling component)**.** *Assume Assumption 4.1, 4.2, and 4.5 hold. Let $\nu := \min_{y' \neq y} \|\mathbb{E}_{T',X'|y'} f_\theta(T'(X'))\|$. Then, for all $\alpha > 0$,*

$$\max_{y' \neq y} s\left(f_\theta(t(x)), \mathbb{E}_{T',X'|y'} f_\theta(T'(X'))\right) \leq \mathbb{E}_{T'}\left[\frac{1}{\nu\alpha} \log \mathbb{E}_{X'} \exp\left(\alpha s\left(f_\theta(t(x)), f_\theta(T'(X'))\right)\right)\right] + \frac{1}{\nu\alpha} \log n. \tag{10}$$

Proof.

$$\max_{y' \neq y} s\left(f_\theta(t(x)), \mathbb{E}_{T',X'|y'} f_\theta(T'(X'))\right) \overset{(i)}{=} \max_{y' \neq y} \frac{f_\theta(t(x)) \cdot \mathbb{E}_{T',X'|y'} f_\theta(T'(X'))}{\|f_\theta(t(x))\| \|\mathbb{E}_{T',X'|y'} f_\theta(T'(X'))\|} \tag{31}$$

$$\overset{(ii)}{=} \max_{y' \neq y} \frac{f_\theta(t(x)) \cdot \mathbb{E}_{T',X'|y'} f_\theta(T'(X'))}{\|\mathbb{E}_{T',X'|y'} f_\theta(T'(X'))\|} \tag{32}$$

$$\overset{(iii)}{\leq} \frac{1}{\nu} \max_{y' \neq y} \mathbb{E}_{T',X'|y'} s\left(f_\theta(t(x)), f_\theta(T'(X'))\right) \tag{33}$$

where (i) is by Assumption 4.1, (ii) is by Assumption 4.2, and (iii) is by the following argument.

Let y^* be the label that achieves the maximum in Equation (32). Note that under Assumption 4.2, $0 < \|\mathbb{E}_{T',X'|y'} f_\theta(T'(X'))\| \leq 1$. If in an ideal case, $f_\theta(t'(x'))$ produces the same representation for every $t'(x')$ that shares the same label y', then $\|\mathbb{E}_{T',X'|y'} f_\theta(T'(X'))\| = \|f_\theta(t'(x'))\| = 1$. To show (iii), we proceed by considering the following two cases.

Case 1: If $f_\theta(t(x)) \cdot \mathbb{E}_{T',X'|y^*} f_\theta(T'(X')) \leq 0$, then

$$\frac{f_\theta(t(x)) \cdot \mathbb{E}_{T',X'|y*} f_\theta(T'(X'))}{\|\mathbb{E}_{T',X'|y*} f_\theta(T'(X'))\|} \overset{(i)}{\leq} \frac{f_\theta(t(x)) \cdot \mathbb{E}_{T',X'|y*} f_\theta(T'(X'))}{\mathbb{E}_{T',X'|y*} \|f_\theta(T'(X'))\|} \tag{34}$$

$$\overset{(ii)}{=} f_\theta(t(x)) \cdot \mathbb{E}_{T',X'|y*} f_\theta(T'(X')) \tag{35}$$

$$\overset{(iii)}{=} \mathbb{E}_{T',X'|y*} s(f_\theta(t(x)), f_\theta(T'(X'))) \tag{36}$$

$$\leq \max_{y' \neq y} \mathbb{E}_{T',X'|y'} s(f_\theta(t(x)), f_\theta(T'(X'))) \tag{37}$$

$$\overset{(iv)}{\leq} \frac{1}{\nu} \max_{y' \neq y} \mathbb{E}_{T',X'|y'} s(f_\theta(t(x)), f_\theta(T'(X'))) \tag{38}$$

where (i) is by Jensen's inequality, (ii) is by Assumption 4.2, (iii) is by a similar argument in the proof of Theorem 4.4, and (iv) follows from the fact that $0 < \nu \leq 1$.

Case 2: If $f_\theta(t(x)) \cdot \mathbb{E}_{T',X'|y^*} f_\theta(T'(X')) > 0$, then

$$\frac{f_\theta(t(x)) \cdot \mathbb{E}_{T',X'|y*} f_\theta(T'(X'))}{\|\mathbb{E}_{T',X'|y*} f_\theta(T'(X'))\|} \overset{(i)}{\leq} \max_{y' \neq y} \frac{1}{\|\mathbb{E}_{T',X'|y'} f_\theta(T'(X'))\|} \max_{y' \neq y} \left[f_\theta(t(x)) \cdot \mathbb{E}_{T',X'|y'} f_\theta(T'(X')) \right] \tag{39}$$

$$= \frac{1}{\nu} \max_{y' \neq y} \left[f_\theta(t(x)) \cdot \mathbb{E}_{T',X'|y'} f_\theta(T'(X')) \right] \tag{40}$$

$$\overset{(ii)}{=} \frac{1}{\nu} \max_{y' \neq y} \mathbb{E}_{T',X'|y'} s(f_\theta(t(x)), f_\theta(T'(X'))) \tag{41}$$

where (i) is by Lemma A.3, and (ii) is by a similar argument in the proof of Theorem 4.4.

Now for brevity, let $g(T'(X')) := s\left(f_\theta(t(x)), f_\theta(T'(X'))\right)$. Then,

$$\max_{y' \neq y} \mathbb{E}_{T',X'|y'} g(T'(X')) \overset{(i)}{\leq} \frac{1}{\alpha} \log \sum_{y' \neq y} \exp\left(\alpha \mathbb{E}_{T',X'|y'} g(T'(X'))\right) \tag{42}$$

$$\overset{(ii)}{\leq} \frac{1}{\alpha} \log \sum_{y'} \exp\left(\alpha \mathbb{E}_{T',X'|y'} g(T'(X'))\right) \tag{43}$$

$$= \frac{1}{\alpha} \log \sum_{y'} \exp\left(\alpha \mathbb{E}_{T'} \mathbb{E}_{X'|y'} g(T'(X'))\right) \tag{44}$$

$$\overset{(iii)}{\leq} \mathbb{E}_{T'} \left[\frac{1}{\alpha} \log \sum_{y'} \exp\left(\alpha \mathbb{E}_{X'|y'} g(T'(X'))\right) \right] \tag{45}$$

$$\overset{(iv)}{\leq} \mathbb{E}_{T'} \left[\frac{1}{\alpha} \log \sum_{y'} \mathbb{E}_{X'|y'} \exp\left(\alpha g(T'(X'))\right) \right] \tag{46}$$

$$\overset{(v)}{=} \mathbb{E}_{T'} \left[\frac{1}{\alpha} \log \left(n \sum_{y'} p(y') \mathbb{E}_{X'|y'} \exp\left(\alpha g(T'(X'))\right) \right) \right] \tag{47}$$

$$= \mathbb{E}_{T'} \left[\frac{1}{\alpha} \log \left(n \mathbb{E}_{Y'} \mathbb{E}_{X'|Y'} \exp\left(\alpha g(T'(X'))\right) \right) \right] \tag{48}$$

$$= \mathbb{E}_{T'} \left[\frac{1}{\alpha} \log \left(n \mathbb{E}_{X'} \exp\left(\alpha g(T'(X'))\right) \right) \right] \tag{49}$$

$$= \mathbb{E}_{T'} \left[\frac{1}{\alpha} \log \left(\mathbb{E}_{X'} \exp\left(\alpha g(T'(X'))\right) \right) \right] + \frac{1}{\alpha} \log n. \tag{50}$$

where (i) is by Lemma A.1, (ii) is by the positivity of $\exp(\alpha x)$ and the monotonicity of $\log(x)$, (iii) is by Lemma A.2 and Jensen's inequality, (iv) is by the convexity of $\exp(\alpha x)$, Jensen's inequality, and the monotonicity of $\log(x)$, and (v) is by Assumption 4.5. This completes the proof of Theorem 4.6. □

A.2 CROSS-REFERENCE

Table 2 shows how each component of SimCLR corresponds to specific parts of our problem formulation and theoretical derivation.

Table 2: Cross-reference between SimCLR and our framework.

Component	SimCLR	Our framework
Architecture	Siamese network	Subsection 4.1 and 4.2
Loss	NT-Xent	Subsection 4.3
Data augmentation	debiased prototype representation	Subsection 3.2
Similarity measure	cosine similarity with normalization	Theorem 4.4 and 4.6
Dataset	balanced	Theorem 4.6

A.3 IMPLEMENTATION DETAILS

This subsection offers a comprehensive description of the implementation details for our experiments. Readers can also refer to the code provided in the supplementary material. With 8 NVIDIA V100 GPUs, the pretraining takes about 2.5 days and 13 GB peak memory usage, the linear evaluation takes about 1.5 days and 8 GB peak memory usage, and the k-nearest neighbors takes about 40 minutes and 30 GB peak memory usage.

A.3.1 BASE SETTING

Dataset We use ImageNet as the benchmark dataset, as it is one of the most representative large-scale image datasets. The training set comprises 1,281,167 images, while the validation set comprises 50,000 images. As ImageNet's test set labels are unavailable, we utilize the validation set as a test set for evaluation purposes. ImageNet encompasses 1,000 classes.

Data augmentation The following data transformations are sequentially applied during pretraining. Due to variations in image sizes, they are first cropped to dimensions of 224×224.

- `RandomResizedCrop`: Randomly crop a patch of the image within the scale range of $(0.2, 1)$, then resize it to dimensions of $(224, 224)$.
- `ColorJitter`: Change the image's brightness, contrast, saturation, and hue with strengths of $(0.4, 0.4, 0.4, 0.1)$ with a probability of 0.8.
- `RandomGrayscale`: Convert the image to grayscale with a probability of 0.2.
- `GaussianBlur`: Apply the Gaussian blur filter to the image with a radius sampled uniformly from the range $[0.1, 2]$ with a probability of 0.5.
- `RandomHorizontalFlip`: Horizontally flip the image with a probability of 0.5.
- `Normalize`: Normalize the image using a mean of $(0.485, 0.456, 0.406)$ and a standard deviation of $(0.229, 0.224, 0.225)$.

Network architecture The encoder consists of a backbone followed by a projector. We employ ResNet-50 as the backbone and a three-layered fully-connected MLP as the projector. For the projector, the input and output dimensions of all layers are set to 2,048. Batch normalization (Ioffe & Szegedy, 2015) is applied to all layers, and the ReLU activation function is applied to the first two layers.

Pretraining configuration We pretrain the encoder with a batch size of 512 for 100 epochs. We employ the SGD optimizer and set the momentum to 0.9, the learning rate to 0.1, and the weight decay rate to 0.0001. Additionally, we implement a cosine decay schedule for the learning rate, as proposed by Loshchilov & Hutter (2016); Chen et al. (2020a).

Evaluation configuration After pretraining, we employ linear evaluation, which is the standard evaluation protocol. We take and freeze the pretrained backbone and attach a linear classifier on top. The linear classifier is then trained on the training set and evaluated on the test set. Training the linear classifier is conducted with a batch size of 4,096 for 90 epochs, utilizing the LARS optimizer (You et al., 2017).

A.3.2 Implementation details for Section 5.3

To estimate the value of the prototype representation bias, for each (x_i, y_i) in the ImageNet training set $\mathcal{D}$, we sample t_i from T and x_i' from $X|y_i$ and calculate the deviation $\|f_\theta(t_i(x_i')) - f_\theta(t_i(x_i))\|$. Then, we take the average over the entire $\mathcal{D}$ as follows:

$$\frac{1}{|\mathcal{D}|} \sum_{(x_i, y_i) \in \mathcal{D}} \|f_\theta(t_i(x_i')) - f_\theta(t_i(x_i))\|. \tag{51}$$

So, we consider total 1,281,167 samples, which is equivalent to the number of images in the ImageNet training set.

A.3.3 Implementation details for Section 5.4

When normalization is not carried out, there is a risk of loss overflow, so we resort to using the log-sum-exp trick. It does not alter the values themselves.

A.3.4 Implementation details for Section 5.5

We use ImageNet-LT (ImageNet Long-Tailed) as a benchmark for imbalanced datasets. ImageNet-LT is a representative dataset specifically designed to address the challenges associated with imbalanced datasets. It is subsampled across the 1,000 classes of ImageNet, following a Pareto distribution with a shape parameter α of 6. The training set consists of 115,846 images, which is approximately 9% of the entire ImageNet training set. The class with the most images contains 1,280 images, while the class with the fewest has only 5 images. The test set is balanced, consisting of 50,000 images, with each class having exactly 50 images.

We construct ImageNet-Uni (ImageNet Uniform) as a subset of ImageNet to enable a fair comparison. We uniformly sample 115,846 images from the ImageNet training set, matching the size of the ImageNet-LT training set. The test set is configured to be identical to that of ImageNet-LT.

A.4 Further experiments

In this subsection, we provide additional experimental results. We include results on CIFAR-10 (Krizhevsky et al., 2009). Note that, since CIFAR-10 contains 10 classes, the chance-level accuracy is 10%.

A.4.1 Implementation details for CIFAR-10 experiments

Dataset The training set comprises 60,000 images, while the test set comprises 10,000 images. CIFAR-10 contains 10 classes, with all images standardized to a fixed size of 32×32.

Data augmentation The following data transformations are sequentially applied during pretraining.

- `RandomResizedCrop`: Randomly crop a patch of the image within the scale range of $(0.08, 1)$, then resize it to dimensions of $(32, 32)$.
- `RandomHorizontalFlip`: Horizontally flip the image with a probability of 0.5.
- `ColorJitter`: Change the image's brightness, contrast, saturation, and hue with strengths of $(0.4, 0.4, 0.4, 0.1)$ with a probability of 0.8.
- `RandomGrayscale`: Convert the image to grayscale with a probability of 0.2.
- `Normalize`: Normalize the image using a mean of $(0.485, 0.456, 0.406)$ and a standard deviation of $(0.229, 0.224, 0.225)$.

Table 3: Standard evaluations.

Dataset	Protocol	
	k-NN	Linear eval.
CIFAR-10	80.32 ± 0.32	86.08 ± 0.07
ImageNet	51.00 ± 0.22	67.40 ± 0.07

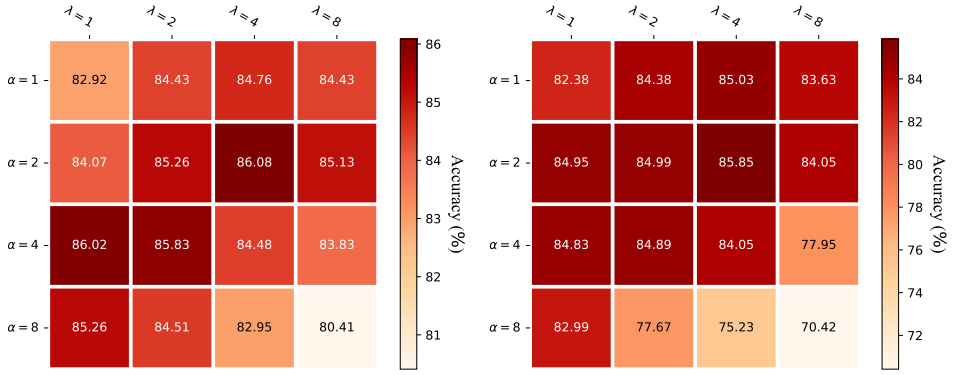

(a) Balanced contrastive loss (b) Generalized NT-Xent loss

Figure 5: **Impact of balancing parameters α and λ.** Better balancing can be accomplished through the adjustments of the balancing parameters.

Network architecture The encoder consists of a backbone followed by a projector. We employ a variant of ResNet-18 for CIFAR-10 as the backbone and a two-layered fully-connected MLP as the projector. For the projector, the input and output dimensions of the first layer and 512 and 2,048, respectively, and the input and output dimensions of the second layer are 2,048. Batch normalization is applied to all layers, and the ReLU activation function is applied to the first layer.

Pretraining configuration We pretrain the encoder with 512 batch size for 200 epochs. We employ the SGD optimizer and set the momentum to 0.9, the learning rate to 0.1, and the weight decay rate to 0.0001.

Evaluation configuration Training the linear classifier is conducted with a batch size of 256 over 90 epochs, utilizing the SGD optimizer. We set the momentum to 0.9 and learning rate to 30 and use a cosine decay schedule.

A.4.2 Standard evaluations

Table 3 presents a set of standard evaluations. Error bars, represented as the mean $\pm$ standard deviation, are reported based on five independent runs. We choose (α, λ) as $(4, 2)$ and $(2, 4)$ for ImageNet and CIFAR-10, respectively. We also include k-nearest neighbors evaluation. Specifically, we retrieve the k nearest training image representations for a given test image representation. Their respective labels are aggregated using a majority voting process to predict the label for the test image. In ImageNet experiments, k is set to 200, whereas in CIFAR-10 experiments, k is set to 1.

A.4.3 Impact of balancing parameters on CIFAR-10

As in Section 6, Figure 5 shows that, balancing between the attracting component and the repelling component is important using balancing parameters α and λ.

Table 4: The performance is better when the class distribution is balanced.

Class distribution	
Uniform	Long-tailed
20.82	13.65

A.4.4 EXPERIMENTS ON BALANCED DATASETS

We provide additional evidence in our setting for the sake of completeness. Table 4 displays SimCLR performs better on a balanced dataset compared to an imbalanced one. In both cases, the training sets contain the same number of images (115,846, which is 9% of the ImageNet training set), but they differ in class distribution. We use an identical test set for both cases.